Whole-body and intravital optical imaging of angiogenesis in orthotopically implanted tumors

Meng Yang*, Eugene Baranov*, Xiao-Ming Li*, Jin Wei Wang*, Ping Jiang*, Lingna Li*, A. R. Moossa†, Sheldon Penman‡, and Robert M. Hoffman*†§

*AntiCancer, Inc., 7917 Ostrow Street, San Diego, CA 92111; †Department of Surgery, University of California, 200 West Arbor Drive, San Diego, CA 92103-8220; and ‡Department of Biology, Massachusetts Institute of Technology, 77 Massachusetts Avenue, Cambridge, MA 02139-4307

Contributed by Sheldon Penman, December 28, 2000

The development of drugs for the control of tumor angiogenesis requires a simple, accurate, and economical assay for tumor-induced vascularization. We have adapted the orthotopic implantation model to angiogenesis measurement by using human tumors labeled with *Aequorea victoria* green fluorescent protein for grafting into nude mice. The nonluminous induced capillaries are clearly visible against the very bright tumor fluorescence examined either intravitally or by whole-body luminance in real time. The orthotopic implantation model of human cancer has been well characterized, and fluorescence shadowing replaces the laborious histological techniques for determining blood vessel density. Intravital images of orthotopically implanted human pancreatic tumors clearly show angiogenic capillaries at both primary and metastatic sites. A quantitative time course of angiogenesis was determined for an orthotopically growing human prostate tumor periodically imaged intravitally in a single nude mouse over a 19-day period. Whole-body optical imaging of tumor angiogenesis was demonstrated by injecting fluorescent Lewis lung carcinoma cells into the s.c. site of the footpad of nude mice. The footpad is relatively transparent, with comparatively few resident blood vessels, allowing quantitative imaging of tumor angiogenesis in the intact animal. Capillary density increased linearly over a 10-day period as determined by whole-body imaging. Similarly, the green fluorescent protein-expressing human breast tumor MDA-MB-435 was orthotopically transplanted to the mouse fat pad, where whole-body optical imaging showed that blood vessel density increased linearly over a 20-week period. These powerful and clinically relevant angiogenesis mouse models can be used for real-time *in vivo* evaluation of agents inhibiting or promoting tumor angiogenesis in physiological microenvironments.

green fluorescent protein | metastatic models | external optical imaging

Tumor vascularization or angiogenesis is a critical step in tumor growth, progression, and metastasis. As such, angiogenesis promises a uniquely effective yet remarkably benign target for cancer chemotherapy. A major requirement for the effective discovery of angiogenesis-related drugs is an assay system that is accurate, rapid, and economical. We report a model system that meets these requirements.

The discovery and evaluation of antiangiogenic substances initially relied on *in vivo* methods such as the chorioallantoic membrane assay (1, 2), the monkey iris neovascularization model (3), the disk angiogenesis assay (4), and various models that use the cornea to assess blood vessel growth (5–10). Although they are important for understanding the mechanisms of blood vessel induction, these models did not deal with tumor angiogenesis and are poorly suited to drug discovery.

Subcutaneous tumor xenograft angiogenesis models have been developed to study tumor angiogenesis, but these require cumbersome pathological examination procedures such as histology and immunohistochemistry. Measurements require animal sacrifice and therefore preclude ongoing angiogenesis studies in individual, live, tumor-bearing animals (11–14). Moreover, s.c. xenografts are not ideal models of human disease.

Tumors transplanted in the cornea of the rodents (15–17) and rodent skin-fold window chambers have been used for angiogenesis studies (18–20, 29–32). The cornea and skin-fold chamber models provide a means for studying angiogenesis in living animals. However, quantification requires specialized procedures, and the sites do not represent natural environments for tumor growth. The cornea and skin-fold tumor models do not allow orthotopic and metastatic angiogenesis, which may involve mechanisms of angiogenesis (33) that are qualitatively different from these ectopic models.

A suitable model for drug discovery will accurately represent clinical cancer as well as enable real-time visualization of the angiogenesis process and its inhibition by effective agents. To develop realistic and real-time tumor angiogenesis models, the present study utilizes surgical orthotopic implantation (SOI) metastatic models of human cancer (23). These models place tumors in natural microenvironments and replicate clinical tumor behavior more closely than do ectopic implantation models (23). For these studies the tumors implanted in the orthotopic model have been transduced and selected to strongly express green fluorescent protein (GFP) *in vivo* (23–27).

GFP expression in primary tumors and in their metastases in the mouse models can be detected by an intense fluorescence seen by intravital or by whole-body imaging. The nonluminous angiogenic blood vessels appear as sharply defined dark networks against this bright background. The high image resolution permits quantitative measurements of total vessel length. These genetically fluorescent tumor models allow quantitative optical imaging of angiogenesis *in vivo*. Tumor growth, vascularization, and metastasis can now be followed in real time (21–22).

Materials and Methods

Fluorescence Optical Imaging. A Leica fluorescence stereo microscope model LZ12 equipped with a mercury lamp and a 50-W power supply was used. Selective excitation of GFP was produced through a D425/60 band-pass filter and a 470 DCXR dichroic mirror. Emitted fluorescence was collected through a long-pass filter (GG475; Chroma Technology, Brattleboro, VT) on a Hamamatsu C5810 3-chip cooled color charge-coupled device camera (Hamamatsu Photonics, Bridgewater, NJ). Images were processed for contrast and brightness and analyzed with the use of IMAGE PRO PLUS 3.1 software (Media Cybernetics,

Abbreviations: GFP, green fluorescent protein; SOI, surgical orthotopic implantation.

§To whom reprint requests should be addressed. E-mail: all@anticancer.com.

The publication costs of this article were defrayed in part by page charge payment. This article must therefore be hereby marked "*advertisement*" in accordance with 18 U.S.C. §1734 solely to indicate this fact.

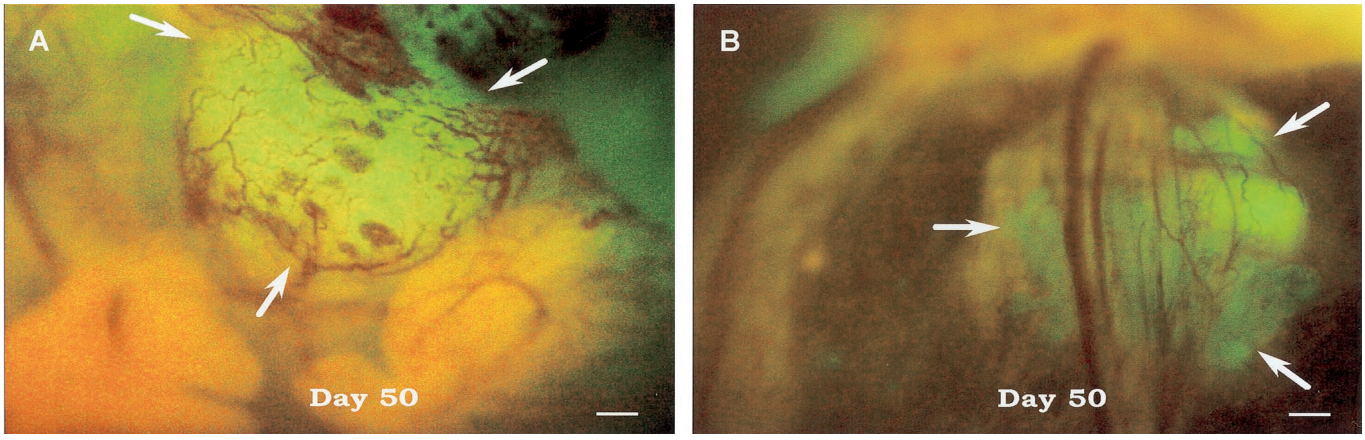

Fig. 1. Intravital fluorescence imaging of Bx-PC-3-GFP human pancreas cancer angiogenesis. (*A*) Orthotopic tumor. (*B*) Metastatic lesion in spleen. The GFP-expressing human tumor was transplanted to nude mice by SOI and intravitally imaged 50 days later, as described in *Materials and Methods*. (Bar = 200 μm.)

Silver Spring, MD). High-resolution images of 1024 × 724 pixels were captured directly on an IBM PC or continuously through video output on a high-resolution Sony VCR (model SLV-R1000; Sony, Tokyo).

Production of GFP Retrovirus. *GFP expression vector.* The pLEIN retroviral vector (CLONTECH) expressing enhanced GFP and the neomycin resistance gene on the same bicistronic message, which contains an internal ribosome entry site (24), was used to transduce tumor cells.

Packaging cell culture, vector production, transfection, and subcloning. PT67, a NIH 3T3-derived packaging cell line expressing the 10 Al viral envelope, was purchased from CLONTECH. PT67 cells were cultured in DMEM (Irvine Scientific) supplemented with 10% heat-inactivated FBS (Gemini Biological Products, Calabasas, CA). For vector production, packaging cells (PT67), at 70% confluence, were incubated with a precipitated mixture of *N*-[1-(2,3-dioleoyloxy)propyl]-*N,N,N*-trimethylammonium methylsulfate reagent (Roche Molecular Biochemicals) and saturating amounts of pLEIN plasmid for 18 h. Fresh medium was replenished at this time. The cells were examined by fluorescence microscopy 48 h after transfection. For selection, the cells were cultured in the presence of 500-2000 mg/ml of G418 (Life Technologies, Grand Island, NY) for 7 days (24).

Retroviral GFP Transduction of Tumor Cells. The cells used were PC-3 human prostate cancer (24), Bx-PC-3 pancreatic cancer (25), MDA-MB-435 human breast cancer (34), and mouse Lewis lung carcinoma (26). For GFP gene transduction, ≈25% confluent cells were incubated with a 1:1 precipitated mixture of retroviral supernatants of PT67 cells and RPMI 1640 (GIBCO) containing 10% FBS (Gemini Biological Products) for 72 h. Fresh medium was replenished at this time. Cells were harvested by trypsin/EDTA 72 h after transduction and subcultured at a ratio of 1:15 into selective medium, which contained 200 mg/ml of G418. The level of G418 was increased stepwise up to 1000 mg/ml for PC-3, 800 mg/ml for Bx-PC-3, 600 mg/ml for MDA MB-435, and 400 mg/ml for Lewis lung carcinoma cells. Clones stably expressing GFP were isolated with cloning cylinders (Bel-Art Products) with the use of trypsin/EDTA and were then amplified and transferred by conventional culture methods.

Animals. All animal studies were conducted in accordance with the principles and procedures outlined in the National Institutes of Health Guide for the Care and Use of Laboratory Animals under assurance number A3873-1. Six-week-old BALB/c *nu/nu* male and female nude mice were used in this study.

SOI of Tumors (23). Tumor fragments (1 mm^3), stably expressing GFP, previously grown s.c. in nude mice, were implanted by SOI on the appropriate organ in nude mice. After proper exposure of the organ to be implanted, 8–0 surgical sutures were used to penetrate the tumor pieces and attach them to the appropriate orthotopic organ. The incision in the skin was closed with a 7–0 surgical suture in one layer. The animals are kept under isoflurane anesthesia during surgery. All procedures of the operation described above were performed with a ×7 magnification microscope (MZ6; Leica, Nussloch, Germany).

Footpad Tumor Implantation. Nude mice were injected s.c. in the footpad with 2×10^4 Lewis lung carcinoma-GFP cells. Cells were first harvested by trypsinization and washed three times with cold serum medium and then injected in a total volume of 10 μl within 40 min of harvesting.

Quantitative Analysis of Angiogenesis. Periodically, the tumor-bearing mice were examined by intravital or whole-body fluorescence imaging. The extent of blood vessel development in a tumor was evaluated based on the total length of blood vessels (L) in chosen areas: areas containing the highest number of vessels were identified by scanning the tumors (28) by intravital or whole-body imaging. To compare the level of vascularization during tumor growth, the "hot" areas with the maximum development of vessels per unit area (35) were then quantitated for L expressed in pixels. Captured images were corrected for unevenness in illumination. Then the total number of pixels derived from the blood vessels was quantified with IMAGE PRO PLUS software.

Results and Discussion

Intravital Images of Angiogenesis of Orthotopic Bx-PC-3-GFP Pancreas Cancer. The clarity of angiogenic blood vessel imaging is illustrated by intravital examination of the orthotopic growth of a Bx-PC-3-GFP pancreatic tumor (Fig. 1*A*). The nonluminous blood vessels are clearly visible against the GFP fluorescence of the primary tumor. Angiogenesis associated with metastatic growths is also easily imaged by intravital examination. Fig. 1*B* shows angiogenesis of a Bx-PC-3-GFP tumor metastasis that has migrated to the spleen.

Intravital Imaging of Angiogenesis of Orthotopic PC-3-GFP Prostate Tumor. Because angiogenesis can now be measured without animal sacrifice, it is possible determine a time course for

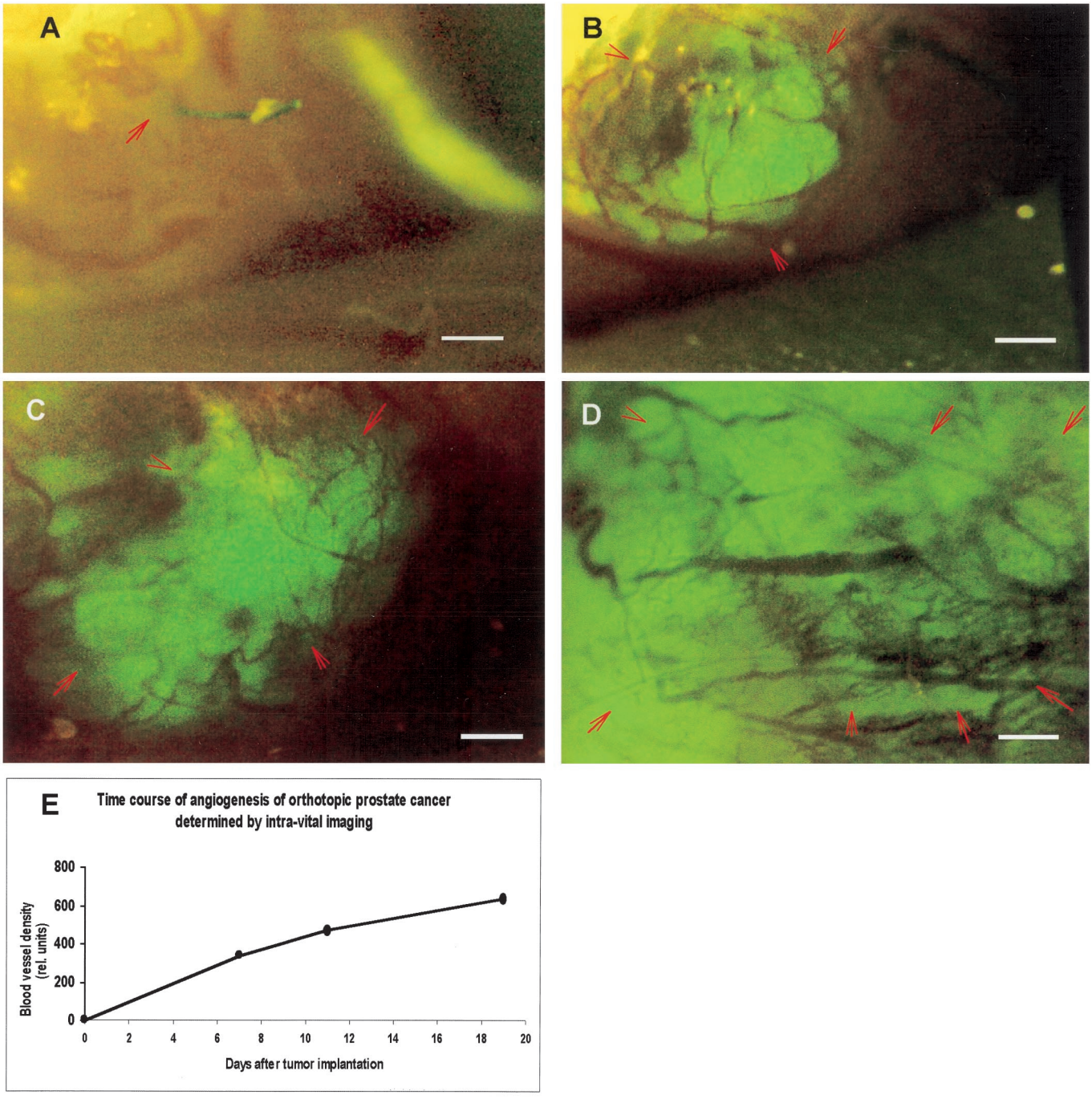

Fig. 2. Time course of intravital fluorescence imaging of PC-3-GFP human prostate cancer angiogenesis in orthotopic primary tumor. The GFP-expressing human tumor was transplanted to nude mice by SOI and imaged as described in *Materials and Methods*. (*A*) Day 1. (*B*) Day 7. (*C*) Day 11. (*D*) Day 19. (*E*) Quantitative graph of microvessel density as function of time. (Bar = 470 μm.)

individual animals. Fig. 2 shows sequential intravital images of angiogenesis for the human prostate tumor PC-3-GFP growing orthotopically in a single nude mouse. The tumor-associated blood vessels are clearly visible by day 7 and continue to increase at least until day 19.

Whole-Body Imaging of Angiogenesis of the Lewis Lung Carcinoma-GFP in the Mouse Footpad. Where possible, the most rapid, least invasive measurement is whole-body optical imaging. Fig. 3 *A–D* comprises whole-body optical images of the Lewis lung carcinoma-GFP growing in the footpad of a nude mouse. The footpad was chosen for its relative transparency and comparatively few resident blood vessels. The onset of tumor angiogenesis and its progression over a 10-day period are clearly imaged in a completely noninvasive manner.

Whole-Body Imaging of Angiogenesis in MDA-MB-435-GFP Breast Cancer Growing Orthotopically in the Breast Fat Pad. Fig. 4 demonstrates the whole-body images and quantitation of the time course of angiogenesis of the MDA-MB-435-GFP human breast cancer growing orthotopically in the breast fat pad in a nude mouse. The development of the tumor and its angiogenesis could be imaged in a completely noninvasive manner.

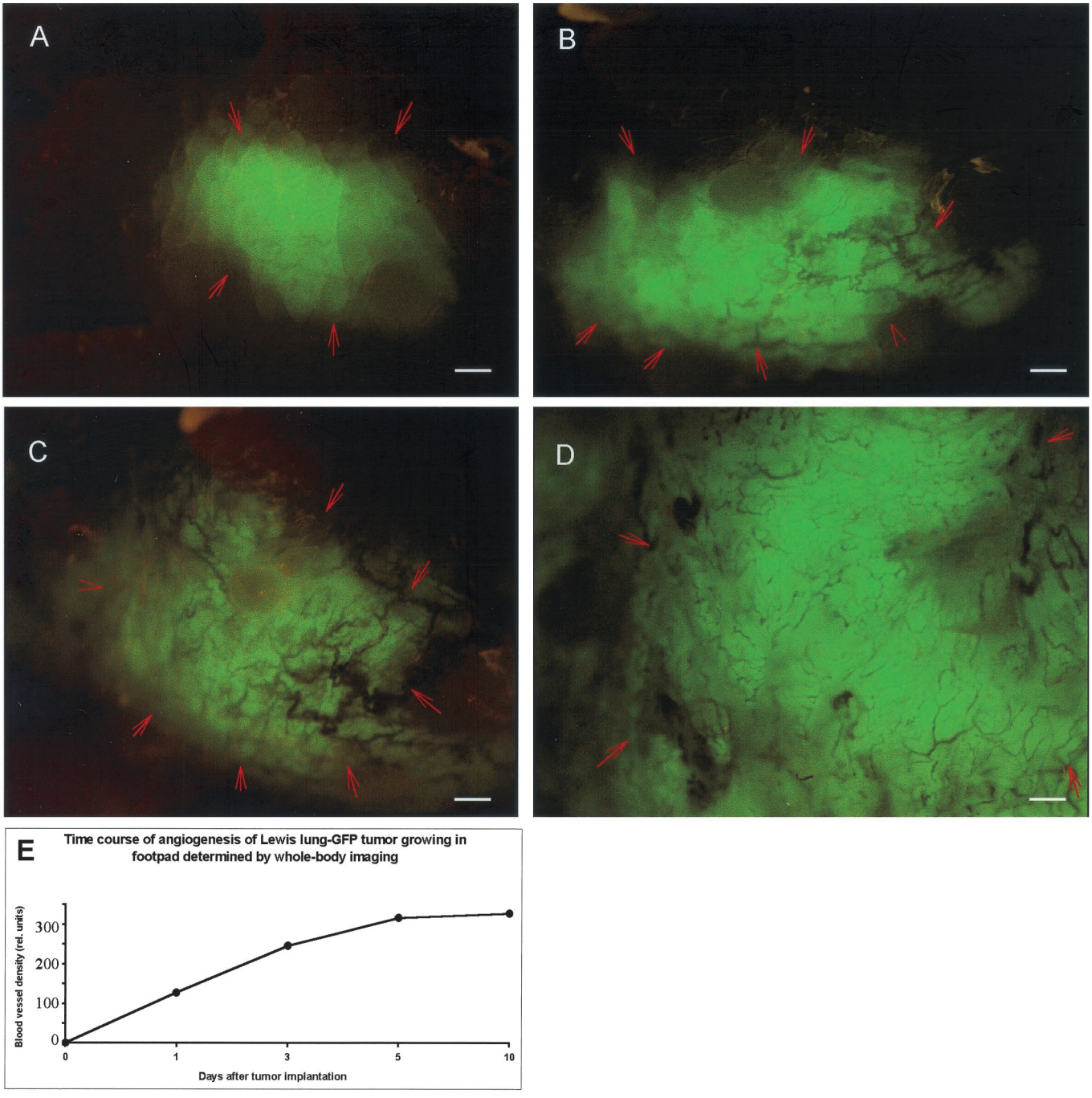

Fig. 3. Time course of whole-body fluorescence imaging of Lewis lung carcinoma-GFP angiogenesis in the mouse footpad. The GFP-expressing tumor cells were injected into the footpad of nude mice and whole-body imaged as described in *Materials and Methods*. (*A*) Day 3. (*B*) Day 6. (*C*) Day 8. (*D*) Day 13. (*E*) Quantitative graph of microvessel density as a function of time. (Bar = 500 μm.)

Quantitative Determination of Angiogenesis. The well-resolved, high-contrast images of tumor-associated blood vessels afforded by high-GFP-expression tumor cells allows real-time quantitative measurements of angiogenesis *in vivo*. The quantitative data obtained by intravital examination of the PC-3-GFP prostate tumor (Fig. 2*E*) show an increase in vessel density over 20 days. These demonstrate quantifying angiogenesis of internally growing, orthotopic tumors without sacrificing the animal.

A wholly noninvasive, quantitative measurement of angiogenesis is possible at sites such as the mouse foot pad. The tissue is relatively transparent, with few endogenous blood vessels. The increase in vessel density of the Lewis lung carcinoma-GFP was quantified from whole-body images over 10 days (Fig. 3*E*). The sensitivity of the method is shown by detection of Lewis lung carcinoma-GFP angiogenesis at high resolution as early as 3 days after implantation (Fig. 3*A*).

The mouse breast fat pad is the orthotopic environment for the implanted MDA-MB-435-GFP breast cancer and allows noninvasive, whole-body imaging of tumor angiogenesis. The quantitative angiogenesis data show that microvessel density increased over 20 weeks (Fig. 4*E*). Thus, tumors, even in their natural microenvironment, growing orthotopically in sites such

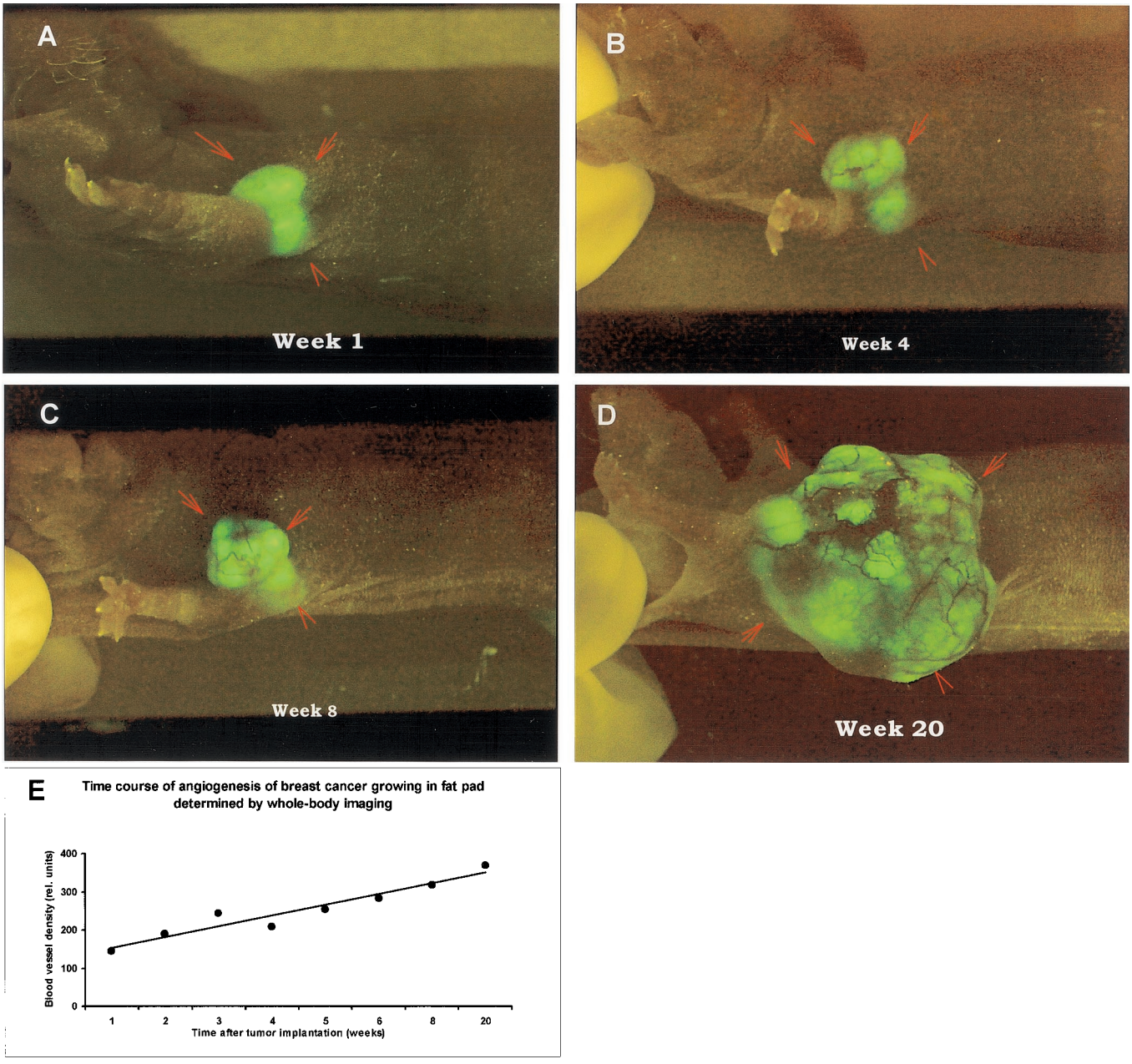

Fig. 4. Time course of whole-body fluorescence imaging of MDA-MB-435-GFP human breast cancer angiogenesis in orthotopic primary tumor. The GFP-expressing human tumor was transplanted by SOI in the fat pad of nude mice and whole-body imaged as described in *Materials and Methods*. (*A*) Week 1. (*B*) Week 4. (*C*) Week 8. (*D*) Week 20. (*E*) Quantitative graph of microvessel density as a function of time.

as the fatpad and presumably others, can be whole-body imaged for quantitative angiogenesis studies.

Comparative Advantages of Fluorescent Tumor Imaging. The present tumor angiogenesis models shown here have many advantages over the traditional tumor angiogenesis models such as the chicken chorioallantoic membrane assay (1, 2), rabbit cornea (5–10), skin-fold window (18–20, 29–32), and s.c. implantation (11–14). These sites are not normal sites for tumor growth, and their microenvironments are very different from orthotopic sites with regard to regulation not only of tumor growth but of the angiogenesis process itself (33). Furthermore, without a marker such as GFP, any type of visualization of angiogenesis requires animal sacrifice and cumbersome preparatory histological and histochemical procedures, ruling out any type of noninvasive real-time studies.

Orthotopically implanted GFP-labeled tumors also allow the study of angiogenesis for metastasis. The orthotopically growing tumors, in contrast to most other models, give rise to spontaneous metastases that resemble, both in target tissues and in frequency of occurrence, the clinical behavior of the original human tumor (23). Moreover, the extreme detection sensitivity afforded by the strong GFP fluorescence allows imaging of very early events in blood vessel induction. As Li *et al.* (30) point out, angiogenesis initiation in metastatic tumors may be very different from that of primary tumors and require different interventions. They used skin-fold chambers with a transparent window for studies of early events in rodent tumor models, including

those expressing GFP (30, 32). Although these afforded a high detection sensitivity and allowed imaging of early angiogenic events, these were not actual metastases, and the ectopic microenvironment can be far from physiological.

The models for whole-body and intravital imaging of angiogenesis of human tumors described here enable the angiogenesis process to be visualized in real time at orthotopic sites, allowing relevant mechanistic studies. The whole-body imaging models will be of particular value for *in vivo* screening and evaluation of antiangiogenesis drugs.

1. Auerbach, R., Kubai, L., Knighton, D. & Folkman, J. (1974) *Dev. Biol.* **41,** 391–394.
2. Crum, R., Szabo, S. & Folkman, J. (1985) *Science* **230,** 1375–1378.
3. Miller, J. W., Stinson, W. G. & Folkman, J. (1993) *Ophthalmology* **100,** 9–14.
4. Passaniti, A., Taylor, R. M., Pili, R., Guo, Y., Long, P. V., Haney, J. A., Pauly, R. R., Grant, D. S. & Martin, G. R. (1992) *Lab. Invest.* **67,** 519–528.
5. Alessandri, G., Raju, F. & Gullino, P. M. (1983) *Cancer Res.* **43,** 1790–1797.
6. Deutsch, T. A. & Hughes, W. F. (1979) *Am. J. Ophthalmol.* **87,** 536–540.
7. Korey, M., Peyman, G. A. & Berkowitz, R. (1977) *Ann. Ophthalmol.* **9,** 1383–1387.
8. Mahoney, J. M. & Waterbury, L. D. (1985) *Curr. Eye Res.* **4,** 531–535.
9. Li, W. W., Grayson, G., Folkman, J. & D'Amore, P. A. (1991) *Invest. Ophthalmol. Vis. Sci.* **32,** 2906–2911.
10. Epstein, R. J., Hendricks, R. L. & Stulting, R. D. (1990) *Cornea* **9,** 318–323.
11. O' Reilly, M. S., Boehm, T., Shing, Y., Fukai, N., Vasios, G., Lane, W. S., Flynn, E., Birkhead, J. R., Olsen, B. R. & Folkman, J. (1997) *Cell* **88,** 277–285.
12. Drevs, J., Hofmann, I., Hugenschmidt, H., Wittig, C., Madjar, H., Muller, W., Wood, J., Martiny-Baron, G., Unger, C. & Marme, D. (2000) *Cancer Res.* **60,** 4819–4824.
13. Prewett, M., Huber, J., Li, Y., Santiago, A., O'Connor, W., King, K., Overholser, J., Hooper, A., Pytowski, B., Witte, L., *et al.* (1999) *Cancer Res.* **59,** 5209–5218.
14. Kurebayashi, J., Kunisue, H., Yamamoto, S., Kurosumi, M., Otsuki, T. & Sonoo, H. (2000) *Oncology* **59,** 158–165.
15. Gimbrone, M. A., Cotran, I. S., Leapman, S. B. & Folkman, J. (1974) *J. Natl. Cancer Inst.* **54,** 413–427.
16. Fournier, G. A., Lutty, G. A., Watt, S., Fenselau, A. & Patz, A. (1981) *Invest. Ophthalmol. Vis. Sci.* **21,** 351–354.
17. Muthukkaruppan, V. & Auerbach, R. (1979) *Science* **205,** 1416–1418.
18. Papenfuss, H. D., Gross, J. F., Intaglietta, M. & Treese, F. A. (1979) *Microvasc. Res.* **18,** 311–318.
19. Gross, J., Roemer, R., Dewhirst, M. & Meyer, T. (1982) *Int. J. Heat Mass Transfer* **25,** 1313–1320.
20. Dewhirst, M., Gross, J., Sim, D., Arnold, P. & Boyer, D. (1984) *Biorheology* **21,** 539–558.
21. Yang, M., Baranov, E., Jiang, P., Sun, F.-X., Li, X.-M., Li, L., Hasegawa, S., Bouvet, M., Al-Tuwaijri, M., Chishima, T., *et al.* (2000) *Proc. Natl. Acad. Sci. USA* **97,** 1206–1211.
22. Yang, M., Baranov, E., Moossa, A. R., Penman, S. & Hoffman, R. M. (2000) *Proc. Natl. Acad. Sci. USA* **97,** 12278–12282.
23. Hoffman, R. M. (1999) *Investigational New Drugs* **17,** 343–359.
24. Yang, M., Jiang, P., Sun, F. X., Hasegawa, S., Baranov, E., Chishima, T., Shimada, H., Moossa, A. R. & Hoffman, R. M. (1999) *Cancer Res.* **59,** 781–786.
25. Bouvet, M., Yang, M., Nardin, S., Wang, X., Jiang, P., Baranov, E., Moossa, A. R. & Hoffman, R. M. (2001) *Clin. Exp. Metastasis*, in press.
26. Rashidi, B., Yang, M., Jiang, P., Baranov, E., An, Z., Wang, X., Moossa, A. R. & Hoffman, R. M. (2000) *Clin. Exp. Metastasis* **18,** 57–60.
27. Chishima, T., Miyagi, Y., Wang, X., Yamaoka, H., Shimada, H., Moossa, A. R. & Hoffman, R. M. (1997) *Cancer Res.* **57,** 2042–2047.
28. Takahashi, Y., Kitadai, Y., Bucana, C. D., Cleary, K. R. & Ellis, L. M. (1995) *Cancer Res.* **55,** 3964–3968.
29. Fukumura, D., Xavier, R., Sugiura, T., Chen, Y., Park, E. C., Lu, N., Selig, M., Nielsen, G., Taksir, T., Jain, R. K., *et al.* (1998) *Cell* **94,** 715–725.
30. Li, C. Y., Shan, S., Huang, Q., Braun, R. D., Lanzen, J., Hu, K., Lin, P. & Dewhirst, M. W. (2000) *J. Natl. Cancer Inst.* **92,** 143–147.
31. Al-Mehdi, A. B., Tozawa, K., Fisher, A. B., Shientag, L., Lee, A. & Muschel, R. J. (2000) *Nat. Med.* **6,** 100–102.
32. Huang, Q., Shan, S., Braun, R. D., Lanzen, J., Anyrhambatla, G., Kong, G., Borelli, M., Corry, P., Dewhirst, M. W. & Li, C. Y. (1999) *Nat. Biotechnol.* **17,** 1033–1035.
33. Cowen, S. E., Bibby, M. C. & Double, J. A. (1995) *Acta Oncol.* **34,** 357–360.
34. Bagheri-Yarmand, R., Kourbali, Y., Rath, A. M., Vassy, R., Martin, A., Jozefonvicz, J., Soria, C., Lu, H. & Crepin, M. (1999) *Cancer Res.* **59,** 507–510.
35. Van Der Laak, J. A., Westphal, J. R., Schalkwijk, L. J., Pahlplatz, M. M., Ruiter, D. J., De Waal, R. M. & De Wilde, P. C. (1998) *J. Pathol.* **184,** 136–143.